Journal of
Materials Chemistry A

Materials for energy and sustainability

Accepted Manuscript

This article can be cited before page numbers have been issued, to do this please use: Z. Tao, T. Sun, C. Liu, X. Xu, Q. Nian, S. Zheng, X. Hou and J. Liang, *J. Mater. Chem. A*, 2020, DOI: 10.1039/D0TA09316E.

ROYAL SOCIETY OF CHEMISTRY

rsc.li/materials-a

View Article Online
DOI: 10.1039/D0TA09316E

COMMUNICATION

Insights on the Hydronium-ions Storage of Alloxazine in mild electrolyte

Received 00th January 20xx,
Accepted 00th January 20xx

DOI: 10.1039/x0xx00000x

Tianjiang Sun,[a] Chang Liu,[a] XiuFang Xu,[a] Qingshun Nian,[a] Shibing Zheng,[a] Xuesen Hou,[a] Jing Liang,[a] Zhanliang Tao*[a]

Here, it is shown for the first time that the alloxazine (ALO) can reversibly store hydronium ions in 1 M $Mg(NO_3)_2$ electrolyte. Comprehensive analysis confirms that the Mg^{2+} ions, with catalysis effect, can promote the hydronium-ions transfer by forming a stable complex with reducing ALO.

Rechargeable batteries have gained great attention in the energy storage system own to the low cost, flexible operationality and sustainability.[1, 2] To date, the charge carrier of rechargeable batteries mainly focus on metal ions, includes Li^+, Na^+, K^+, Zn^{2+}, Mg^{2+}, Ca^{2+} and Al^{3+} ions.[3-10] Among them, lithium ion batteries (LIBs) have been commercialized due to the low weight and high energy density of Li metal, but the limited natural resource and increasing price of Li metal hinder its further development.[11-13] Moreover, it is difficult for other metal ion batteries to surpass LIBs in a short time own to the larger ionic radius, high mass, and/or strong electrostatic interaction. Besides metal ion carrier, proton (H^+), with smaller radius and lower weight, can also be used as potential charge carrier in rechargeable batteries.[14, 15] It is worth noting that the hydronium ion (H_3O^+), rather than naked H^+ ion, is used as charge carrier in aqueous electrolyte because of its high dehydration energy (11.66 eV).[16, 17]

Recently, the energy-storage systems based H_3O^+ ion have been achieved in few organic and inorganic materials. For example, Ji reported hydronium-ion battery with perylenetetracarboxylic dianhydride (PTCDA) as anode, which exhibits a specific capacity of 85 mAh g^{-1}.[17] Yan investigated redox reaction of MoO_3 for hydronium-ion storage. The MoO_3 shows an excellent rate performance with a specific capacity of 88 mAh g^{-1} at an ultrahigh rate of 100 C.[18] The reported hydronium-ion battery is based on H_2SO_4 electrolyte with different concentration, but the strong corrosive character of this is inconsistent with the current development concept of green energy.[19] Additionally, for this system, the hydrogen evolution reaction (HER) in acidic electrolyte is more serious than neutral electrolyte, which caused fairly low coulombic efficiency. Another crucial issue is that the pH value of electrolyte will affect the redox potential of anode (Table S1).[20] It will cause the full cells show an unsatisfactory operate voltage, which hinder its practical application. Compared with strong acidic electrolyte, the mild electrolyte will be an ideal candidate due to the merits of low cost, intrinsic safety, and environmentally friendliness. Nevertheless, there are lots of metal ions and few hydrogen ions in the mild electrolyte, the redox reaction mechanism of electrode materials (inorganic and organic materials) is usually referred to as metal-ions de-/intercalation or uptake/removal, which is controlled by both thermodynamics and kinetics. Therefore, finding a suitable material that can reversibility store hydronium ions in matching mild electrolyte has become an urgent problem.

The reported literatures suggest that the Mg^{2+} ion can promote the proton transfer in Flavin molecule in aqueous solution.[21, 22] Meanwhile, the Mg^{2+} ion, as potential ligand, has ability to stabilize the Flavin molecule by forming coordination compound.[23, 24] Inspired by this, we develop hydronium-ion battery based on alloxazine (ALO) anode in mild electrolyte including 1 M $Mg(NO_3)_2$. Benefit from the same characteristic groups as Flavin, the ALO achieves hydronium-ions uptake/removal by coordination/incoordination reaction due to the Mg^{2+}-ions catalysis (Figure 1a). Furthermore, the formation of complex between the charged ALO and Mg^{2+} ions during charging process will stabilize its structure, so that the ALO electrode can obtain excellent electrochemical performance. The as-obtained ALO electrode exhibits a high discharge capacity of 233.6 mAh g^{-1} at 1 C (250 mA g^{-1}). Moreover, the constructed ALO//$MgMn_2O_4$ (MMO) battery achieves an impressive rate performance with discharge capacity of 72 mAh g^{-1} at 100 C and long cycling stability with 80 % capacity retention after 30000 cycles.

ALO is synthesized by a simple one-step reaction at room temperature. The as-obtained ALO is confirmed by nuclear magnetic resonance spectroscopy (NMR) (Figure S1, S2) and Fourier transform infrared spectroscopy (FTIR) (Figure S3). The scanning electron microscopy (SEM) and transmission electron microscopy energy-dispersive X-ray spectroscopy elemental mappings (TEM-EDS) images of ALO in Figure S4 show homogeneous rod morphology. The

[a] Key Laboratory of Advanced Energy Materials Chemistry (Ministry of Education), College of Chemistry, Nankai University, Tianjin 300071, P. R. China. E-mail: taozhl@nankai.edu.cn

Electronic Supplementary Information (ESI) available: [details of any supplementary information available should be included here]. See DOI:10.1039/x0xx00000x

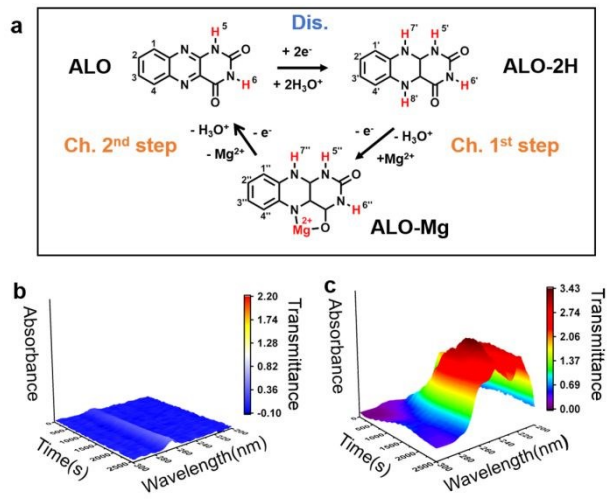

Figure 1. (a) The schematic for reaction mechanism of ALO anode 1 M $Mg(NO_3)_2$ electrolyte (Dis.: Discharge; Ch.: Charge). (b) The in-situ UV-vis spectroscopy of ALO//AC in 1 M $Mg(NO_3)_2$ electrolyte (at a current density of 1 C). (c) The in-situ UV-vis spectroscopy of ALO//AC in 1 M $MgSO_4$ electrolyte (at a current density of 1 C).

termogravimetric analysis (TGA) in Figure S5 shows a good thermostability of ALO.

Different magnesium-containing salt electrolytes are used to study the electrochemical performance of ALO because of the unique effect of Mg^{2+} ion. Unfortunately, the reported ALO material has dissolution problem both in alkaline aqueous and organic electrolytes.[25, 26] To choose a suitable electrolyte with considerable compatibility, the ionic conductivity and solubility tests of ALO in different electrolytes are collected. As shown in Figure S6, the 1 M $Mg(NO_3)_2$ shows impressive ionic conductivity in comparison with other electrolytes (1 M $Mg(CF_3SO_3)_2$, 1 M $MgCl_2$, and 1 M $MgSO_4$). Further, the solubility of ALO in different electrolytes is tested by UV-vis spectroscopy (Figure S7) after standing 24 h (Figure S8). As displayed in Figure S7, the absorption peak at 264 nm corresponds to the signal of ALO.[27, 28] Obviously, the absorption peaks of ALO in 1 M $Mg(NO_3)_2$ and 1 M $MgSO_4$ electrolytes are weaker than others, and the electrolytes still remain clear (Figure S8), indicating that ALO has lower solubility in 1 M $Mg(NO_3)_2$ and 1 M $MgSO_4$ solutions in a resting state. The solubility of ALO can attribute to the different pH of the electrolytes (Figure S9).

To select more suitable electrolyte, the in-situ UV-vis spectroscopy technology is further developed to observe the solubility of ALO during charging/discharging process in 1 M $Mg(NO_3)_2$ and 1 M $MgSO_4$ electrolytes. As shown in Figure 1b, for the cell (ALO//activated carbon (AC)) with 1 M $Mg(NO_3)_2$ solution, only weak absorption peaks are observed, and the peaks hardly strengthen during the charging/discharging process. While the adsorption peaks have gradually increased in 1 M $MgSO_4$ electrolyte (Figure 1c) during charging/discharging process. The analysis of UV-vis patterns indicate the ALO anode is nearly insoluble in 1 M $Mg(NO_3)_2$ electrolyte. Thus, benefit by the high ion conductivity and considerable compatibility with the ALO, 1 M $Mg(NO_3)_2$ electrolyte is more suitable for this system.

To investigated the hydronium-ion uptake/removal performance, the cyclic voltammogram (CV) of ALO is tested in a three-electrode system with 1 M $Mg(NO_3)_2$ electrolyte. As illustrated in Figure 2a, the ALO anode exhibits unsymmetrical redox peaks (two oxidation peaks (-0.52 V and -0.16 V vs Ag/AgCl) and a reduction peak (-0.61 V vs Ag/AgCl) at a scan rate of 0.5 mV s^{-1}), which are different from the reported ALO electrode in other systems (CV curves of reported ALO electrodes are symmetrical).[25, 28-30] The galvanostatic charge-discharge profile of the ALO anode in Figure 2b shows two charge plateaus (a flat plateau and a sloping plateau) and one discharge plateau, which are consist with CV measurement. In addition, the ALO anode achieves a high discharge capacity of 233.6 mAh g^{-1} at 1 C (250 mA g^{-1}), which is close to theoretical specific capacity (250 mAh g^{-1}). Meanwhile, the ALO anode displays an excellent rate performance with a high discharge capacity of 143.6 mAh g^{-1} even at 20 C (5000 mA g^{-1}) (Figure 2c). Based on excellent rate performance, the cycling stability of ALO anode is tested at higher current density. As shown in Figure 2d, the long-term cycle life of ALO anode over 2000 cycles with 80% capacity retention is obtained, which is better than recent reports (Table S2).

To fundamentally understand the reasons of remarkable rate performance of ALO in 1 M $Mg(NO_3)_2$ electrolyte, we investigate the reaction kinetics by CV curves with different scan rates (Figure S10a). The calculated b values of peak 1, peak 2, and peak3 are 0.71, 0.87 and 0.79, respectively, indicating a pseudocapacitive characteristic (Figure S10b). In addition, the hydronium-ion diffusion coefficient on the surface of ALO electrode is tested by CV measurement. As shown in Figure S10c, the diffusion coefficients at Peak 1, Peak 2 and Peak 3 are calculated to be 3.17×10^{-6} cm^2 s^{-1}, 1.42×10^{-6} cm^2 s^{-1} and 1.44×10^{-6} cm^2 s^{-1}, suggesting ultrafast hydronium-ion diffusion. This is one of the reasons for the high rate performance of the ALO electrode.

In-situ pH monitoring technology is carried out to elucidate the hydronium-ion storage mechanism of ALO anode in 1 M $Mg(NO_3)_2$ electrolyte (Figure S11). As shown in Figure 3a, it can be observed that the pH value of the electrolyte increasing during discharging, and gradually decreases during charging. This is due to the reaction

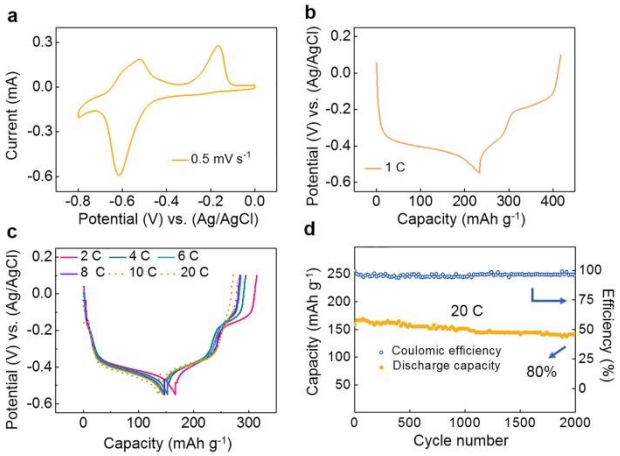

Figure 2. (a) The CV curve of ALO anode at 0.5 mV s^{-1}. (b) The discharge-charge profile of ALO anode at 1 C (250 mA g^{-1}). (c) Rate performance of ALO anode at different current densities from 2 to 20 C. (d) The cycling performance of ALO anode at 20 C (5000 mA g^{-1}).

of hydronium ions with ALO during charging and discharging processes, resulting in a reversible decrease and increase in the concentration of hydrogen ions in the electrolyte and a corresponding change of pH value. Interestingly, the pH value of 1 M $Zn(NO_3)_2$ electrolyte is almost constant during the charging/discharging process, indicating not hydronium ions but zinc ions are de-/insert into ALO electrode (Figure S12), which is consist with the reported literature.[28] Thus, the successful hydronium-ions uptake/removal in ALO suggests that the Mg^{2+} ions, with catalytic effect, promote the hydronium-ions transfer.

To further understand the reaction mechanism of ALO, ex-situ XPS and in-situ FTIR were developed. The XPS spectrum of C 1s is used as a reference (Figure 3b). The XPS spectrum of N 1s and O 1s in Figure 3c and 3d exhibit reversible transformation in different state, suggesting that the group of C=N and C=O are redox-active centers of ALO. In-situ FTIR analysis shown in Figure 3e further confirmed the reversible change in the molecular structure. The peaks at 1658 cm^{-1} (corresponding to the vibrational modes of C=O bond) gradually weaken and enhance during charging/discharging process. While no obvious change about the groups of C=N (at 1581 cm^{-1}) appeared, which may be caused by the weak signal of vibrational modes of C=N. Moreover, the XPS spectrum of Mg 1s are collected in different state. As displayed in Figure 3e, no Mg peak is observed in initial state and discharged state to -0.55 V of the ALO electrode. While the Mg peak appeared when charged to -0.3 V, which implies Mg^{2+} ions may participate in the transformation reaction of ALO anode during charging process.

To confirmed the result, the CV curves of ALO anodes in 1 M $NaNO_3$, 1 M $Zn(NO_3)_2$, and 1 M HNO_3 electrolytes are collected, respectively. As shown in Figure S13, the ALO anodes show a symmetrical redox peaks in 1 M $NaNO_3$, 1 M $Zn(NO_3)_2$, and 1 M HNO_3 electrolytes, which are different from the CV curve of ALO in 1 M $Mg(NO_3)_2$ electrolyte. The result suggests that Mg^{2+} ion selection will alter the electrochemical response of ALO. Moreover, as shown in Figure S14a and 14b, the ALO displays unsymmetrical redox peaks in 1 M $MgSO_4$ electrolyte but symmetrical redox peaks in 1 M $ZnSO_4$ electrolyte, implying that the redox reaction of ALO is independent of the type of anion. The unsymmetrical redox peaks of ALO anode in 1 M $Mg(NO_3)_2$ electrolyte can attribute to the redox reaction including transformation of Mg^{2+} ion with ALO, which is different from reported reaction mechanism about simple metal-ions coordination/incoordination reaction (Li^+, Na^+, and Zn^{2+}).[25, 26, 28]

As the reported literature, ALO molecular structure characterized by the presence of chelation centres mainly located on the groups of C=N and C=O, which can form complex compound between ALO and Mg^{2+} ion.[22, 31] Thus, the reaction mechanism of ALO during charging/discharging process is speculated as below (Figure 1a): When discharging, ALO obtains two electrons and gets two hydronium ions to form ALO-2H, which experiences one-step reaction. Subsequently, ALO-2H first removes a hydronium ion, and is rapidly replaced by Mg^{2+} ion to form ALO-Mg complex during the charging process from -0.55 V to -0.3 V. The substitution process may attribute to the physico-chemical properties of the functional groups and the electron density at the donor atom in ALO molecular, and strong electroaffinity of Mg^{2+} ions. Then the Mg^{2+} ion and hydronium ion are removed to form ALO with continuously charging to 0.1 V, which may be affected by the external electric field.

To improve the understanding on the ions storage mechanism of ALO, density functional theory (DFT) calculations are carried out. As shown in Figure 3g and Table S4, The energies of ALO bonded with one H^+ and two H^+ ions are negative (-7.145 eV and -14.349 eV), indicating the efficient utilization of the nitrogen sites. The ALO transforms into ALO-2H by one-step reaction during discharging process due to the large energy gaps (ΔE = -14.349 eV). During charging process, the energy of ALO-Mg (-11.339 eV) is lower than ALO-H (-7.145 eV), indicating the ALO-2H is more likely become ALO-Mg during the 1st step charging. Then, the ALO-Mg will extract Mg^{2+} and residual H^+ ion and revert to ALO during the 2nd step charging process.

In addition, the ex-situ ^1H NMR is used to study the redox mechanism of ALO (Figure 3h). In the initial state, the chemical shifts of ALO are 7.78 (m, 1H), 7.93 (d, 2H), 8.17 (d, 1H), 11.75 (s, 1H), 11.94 (s, 1H). After discharging to -0.55 V, a new peak, corresponding to two hydrogen ions at 7' and 8' in Figure 3g, suggesting that the ALO transform into ALO-2H during discharge, which also coincided with the discharge capacity. When charged to -0.3 V, the 6' peak shifts to a high field forming 6'' peak, and the peak at 7' 8' weakened into 7'' peak (the area of the 7'' peak is only half that of the 7' 8' peak) and shifted towards the high field, indicating the ALO-2H lose a hydronium ion during the first charging flat (-0.3 V). The shift and weaken of peaks are caused by the extraction of hydronium ion and complex effect of magnesium ion. The analysis about hydrogen numbers and sites is consist well with the molecular structure of ALO-Mg in Figure 3g. Continue to charge to 0.1 V, the ^1H NMR spectrum of the electrode material is the same as that of the original electrode material ALO, indicating the reversibility of charge and discharge of the electrode material. Both analysis of ex-situ XPS and

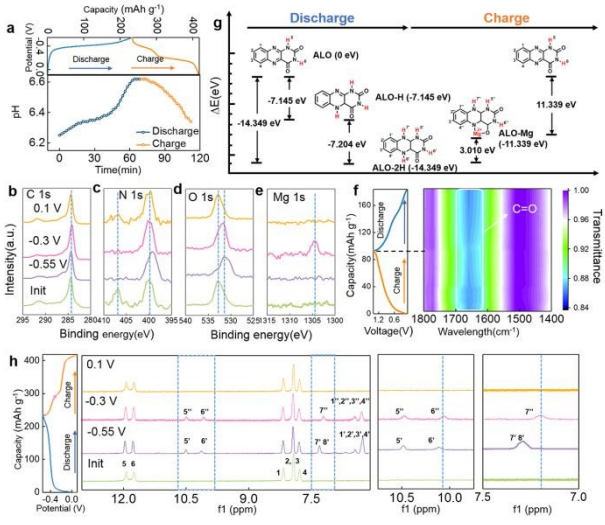

Figure 3. (a) In-situ pH monitor for 1 M $Mg(NO_3)_2$ electrolyte during charging/discharging process (Potential (V vs Ag/AgCl); current density: 1 C). (b~e) Ex-situ XPS spectrum of b) C 1s, c) N 1s, d) O 1s, e) Mg 1s. (f) In-situ FTIR of ALO anode during charging/discharging process. (g) The energy change of ALO during discharging/charging process by DFT calculations. (h) Ex-situ ^1H NMR patterns of ALO anode at different state (Potential (V vs Ag/AgCl); current density: 1 C).

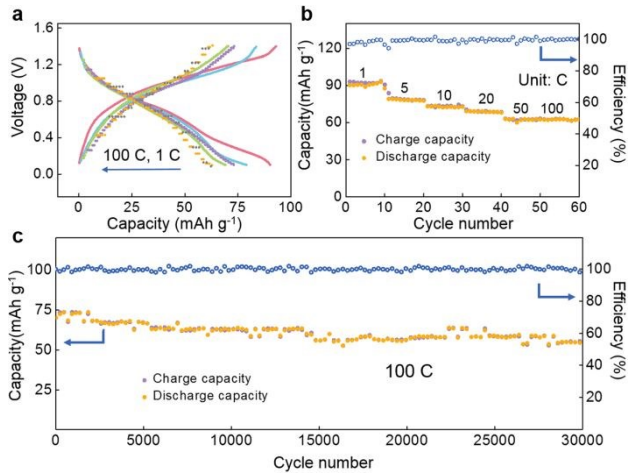

Figure 4. (a) Discharge-charge profiles of full cell of ALO//MMO battery at different current densities of 1, 5, 10, 20, 50, and 100 C (the specific capacity is calculated based on the total mass of active materials in both electrodes). (b) Rate performance of ALO//MMO battery at different current densities of 1, 5, 10, 20, 50, and 100 C. (c) The cycling performance and coulombic efficiencies of ALO//MMO battery at 100 C (25000 mA g^{-1}).

^{1}H NMR patterns are in excellent agreement with the speculation. Benefit by the formation of complex, the ALO electrode shows excellent cycling stability in 1 M $Mg(NO_3)_2$ electrolyte in comparison with in 1 M $Zn(NO_3)_2$ electrolyte (Figure S15).

To further study the practical application prospect of ALO, the $MgMn_2O_4$ (MMO) is used as cathode to construct a full cell. The corresponding synthesis, characterization and electrochemical study are displayed in the supporting information (Figure S16-S19). The full cell, consists of ALO anode, MMO cathode and 1 M $Mg(NO_3)_2$ electrolyte, shows excellent electrochemical performance. As shown in Figure 4a, a discharge capacity of 93 mAh g^{-1} and an energy density of 80 Wh kg^{-1} at 1 C are delivered by this system (calculated based on the total mass of active materials in both electrodes). As shown in Figure 4b, the battery exhibits excellent rate performance with a discharge capacity of 72 mAh g^{-1} even at the high rate of 100 C, which is benefit by the pseudocapacitive characteristic and the high ions diffusion coefficient of ALO anode and MMO cathode. Benefit by the high rate capacity, The ALO//MMO battery is tested at 100 C. As displayed in Figure 4c, the battery achieves a long-life cycling stability with capacity retention of 80% after 30000 cycles, corresponding to a capacity decay of as low as 0.00067% per cycle. The impressive cycling stability of this system is benefit from the insoluble character of ALO and stable structure of MMO in 1M $Mg(NO_3)_2$ electrolyte (Figure S20, S21).

Moreover, the ALO//MMO battery is tested in a wide temperature range from 0 to 70 °C. Electrochemical impedance spectroscopy (EIS) of ALO// MMO battery in Figure S22a shows low charge transfer impedance at different temperatures, suggesting rapid ion diffusion kinetic. Figure S22b shows the charge-discharge profiles of the ALO//MMO battery at different temperatures. The system exhibits 67 % capacity retention at 0 °C in comparison with at 25 °C. Further, this battery shows a good cycling stability with 83% capacity retention after the 1000 cycles at 0 °C, indicating that the ALO//MMO battery can stably operate at a low temperature (Figure S23). Noted that the discharge capacity of this battery is higher at 50 and 70 °C, it reaches 81 mAh g^{-1} and 91 mAh g^{-1}, respectively (Figure S22b). The reason of higher capacity is that higher temperatures improve the ions transport and electronic conductivity of the cathode and anode. In addition, the battery could still maintain a usable capacity of 49 mAh g^{-1} after cycling 10000 cycles at 70 °C, corresponding to a capacity decay of as low as 0.005% per cycle with excellent coulombic efficiency of nearly 99% (Figure S22c). In a word, the ALO//MMO battery represents a balanced and highly competitive capacity retention rate and cycling performance over a wide temperature range from 0 °C to 70 °C.

In conclude, the ALO material is used as anode in hydronium-ion battery. The insoluble character of ALO in 1 M $Mg(NO_3)_2$ electrolyte is confirmed by ex-/in-situ UV-vis spectroscopy technology. Post-mortem analyses including in-situ pH monitor, ex-situ XPS, in-suit FTIR, DFT calculation, along with ex-situ ^{1}H NMR demonstrate the rapid hydronium-ion uptake/removal in ALO. We also confirm the Mg^{2+} ions, with catalytic effect, promote the hydronium-ions transfer in ALO, and the Mg^{2+} ions can form complex with charged ALO to stabilize its structure. The constructed ALO//MMO battery achieves an excellent cycling stability with 80 % capacity retention after 30000 cycles, and remarkable rate performance with considerable discharge capacity of 72 mAh g^{-1} at 100 C. Furthermore, this system is successfully operated at a wide temperature range from 0 to 70 °C and shows significant electrochemical performance. The ALO, with unique reaction mechanism in 1 M $Mg(NO_3)_2$ electrolyte, shows impressive electrochemical performance and can be considered as an ideal anode material for hydronium ion batteries.

Conflicts of interest

"There are no conflicts to declare".

Acknowledgment

This study was supported by the National Key R&D Program of China (2016YFB0901500, 2016YFB0202500 and 2019YFA0705600); the National Natural Science Foundation of China (51771094, 21835004, 21673243 and 52001170), Ministry of Education of China (B12015 and IRT13R30), and Tianjin Natural Science Foundation (No. 18JCZDJC31500).

References

1. C. Han, J. Zhu, C. Zhi and H. Li, J. Mater. Chem. A, 2020, 8, 15479-15512.
2. J. Huang, X. Dong, Z. Guo and Y. Wang, *Angew. Chem. Int. Ed.*, 2020, 2020, **59**, 18322-18333.
3. J. Liu, Z. Bao, Y. Cui, E. J. Dufek, J. B. Goodenough, P. Khalifah, Q. Li, B. Y. Liaw, P. Liu, A. Manthiram, Y. S. Meng, V. R. Subramanian, M. F. Toney, V. V. Viswanathan, M. S. Whittingham, J. Xiao, W. Xu, J. Yang, X.-Q. Yang and J.-G. Zhang, *Nat. Energy*, 2019, **4**, 180-186.

4. H. Gao, I. D. Seymour, S. Xin, L. Xue, G. Henkelman and J. B. Goodenough, *J. Am. Chem. Soc.*, 2018, **140**, 18192-18199.
5. L. Xue, Y. Li, H. Gao, W. Zhou, X. Lu, W. Kaveevivitchai, A. Manthiram and J. B. Goodenough, *J. Am. Chem. Soc.*, 2017, **139**, 2164-2167.
6. Y. Zhang, F. Wan, S. Huang, S. Wang, Z. Niu and J. Chen, *Nat. Commun.*, 2020, **11**, 2199.
7. L. Chen, J. L. Bao, X. Dong, D. G. Truhlar, Y. Wang, C. Wang and Y. Xia, *ACS Energy Lett.*, 2017, **2**, 1115-1121.
8. M. Adil, A. Sarkar, A. Roy, M. R. Panda, A. Nagendra and S. Mitra, *ACS Appl. Mater. Interfaces*, 2020, **12**, 11489-11503.
9. D. J. Kim, D.-J. Yoo, M. T. Otley, A. Prokofjevs, C. Pezzato, M. Owczarek, S. J. Lee, J. W. Choi and J. F. Stoddart, *Nat. Energy*, 2018, **4**, 51-59.
10. D. Wang, L. Wang, G. Liang, H. Li, Z. Liu, Z. Tang, J. Liang and C. Zhi, *ACS Nano*, 2019, **13**, 10643-10652.
11. K. Zhu, T. Wu and K. Huang, *Adv. Energy Mater.*, 2019, **9**, 1901968.
12. X. Wu, Y. Qi, J. J. Hong, Z. Li, A. S. Hernandez and X. Ji, *Angew. Chem. Int. Ed.*, 2017, **56**, 13026-13030.
13. Y. Liu, B. Yang, X. Dong, Y. Wang and Y. Xia, *Angew. Chem. Int. Ed.*, 2017, **56**, 16606-16610.
14. Z. Tie, L. Liu, S. Deng, D. Zhao and Z. Niu, *Angew. Chem. Int. Ed.*, 2020, **59**, 4920-4924.
15. Y. Deng, Z. Cao, L. Wang, Y. Zhou, S. Fu, Y. Peng, Y. Yin, D. Li, W. Wang, W. Zhou and D. Tang, *Solid State Ionics*, 2020, **353**, 115380.
16. Z. Guo, J. Huang, X. Dong, Y. Xia, L. Yan, Z. Wang and Y. Wang, *Nat. Commun.*, 2020, **11**, 959.
17. X. Wang, C. Bommier, Z. Jian, Z. Li, R. S. Chandrabose, I. A. Rodriguez-Perez, P. A. Greaney and X. Ji, *Angew. Chem. Int. Ed.*, 2017, **56**, 2909-2913.
18. X. Wang, Y. Xie, K. Tang, C. Wang and C. Yan, *Angew. Chem. Int. Ed.*, 2018, **57**, 11569-11573.
19. G. Liang, F. Mo, Q. Yang, Z. Huang, X. Li, D. Wang, Z. Liu, H. Li, Q. Zhang and C. Zhi, *Adv. Mater.*, 2019, **31**, 1905873.
20. Z. Liu, Y. Huang, Y. Huang, Q. Yang, X. Li, Z. Huang and C. Zhi, *Chem. Soc. Rev.*, 2020, **49**, 180-232.
21. H. N. Seiji Shinkai, Takaharu Tsuno, Osamu Manabe, Atsuyoshi Ohno, *Chem. Commun.*, 1984, 2, 849-850.
22. S. K. Shunichi FUKUZUMI, Toshio TANAKA, *Chem. Lett.*, 1984, 4, 417-420.
23. B. S. Wolfgang Kaim , Oliver Heilmann,Fridmann M. Hornung, *Coordination Chem. Rev.*, 1998, **182**, 20, 323-342.
24. M. Scheurer, D. Brisker-Klaiman and A. Dreuw, *J. Phys. Chem. B*, 2017, **121**, 10457-10466.
25. L. Zhong, Y. Lu, H. Li, Z. Tao and J. Chen, *ACS Sustainable Chem. Eng.*, 2018, **6**, 7761-7768.
26. J. Hong, M. Lee, B. Lee, D. H. Seo, C. B. Park and K. Kang, *Nat. Commun.*, 2014, **5**, 5335.
27. B. Tian, Z. Ding, G. H. Ning, W. Tang, C. Peng, B. Liu, J. Su, C. Su and K. P. Loh, *Chem. Commun.*, 2017, **53**, 2914-2917.
28. L. Cheng, Y. Liang, Q. Zhu, D. Yu, M. Chen, J. Liang and H. Wang, *Chem. Asian. J.*, 2020, **15**, 1290-1295.
29. K. Lin, R. Gómez-Bombarelli, E. S. Beh, L. Tong, Q. Chen, A. Valle, A. Aspuru-Guzik, M. J. Aziz and R. G. Gordon, *Nat. Energy*, 2016, **1**, 16102.
30. W. Lee, B. W. Kwon and Y. Kwon, *ACS Appl. Mater. Interfaces*, 2018, **10**, 36882-36891.
31. N. O. Obi-Egbedi and I. B. Obot, *Corros. Sci.*, 2011, **53**, 263-275.

View Article Online
DOI: 10.1039/D0TA09316E

Table of Contents

View Article Online
DOI: 10.1039/D0TA09316E

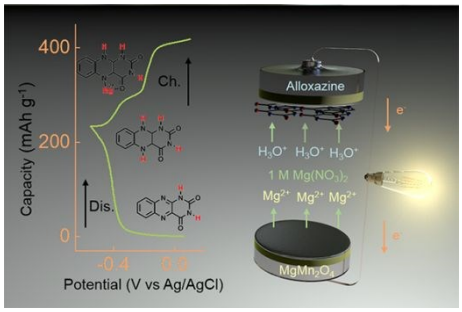

The Mg^{2+}, with catalysis effect, can promote the hydronium ion transfer in alloxazine in 1 M $Mg(NO_3)_2$ electrolyte.